Optimization of a nanotip on a surface for the ultrafast probing of propagating surface plasmons

B. Ahn,[1,2,3] J. Schötz,[3] W. A. Okell,[3] F. Süßmann,[3,4] B. Förg,[3,4] S.C. Kim,[1,2] M.F. Kling,[3,4] and D. Kim[1,2,*]

[1]*Department of Physics, Center for Attosecond Science and Technology, Pohang University of Science and Technology, Pohang, 37673, South Korea*
[2]*Max Planck Center for Attosecond Science, Max Planck POSTECH/KOREA Res. Insit., Pohang, 37673, South Korea*
[3]*Max Planck Institute of Quantum Optics, D-85748 Garching, Germany*
[4]*Physics Department, Ludwig-Maximilians-Universität München, D-85748 Garching, Germany*
[*]*kimd@postech.ac.kr*

Abstract: We theoretically analyze a method for characterizing propagating surface plasmon polaritons (SPPs) on a thin gold film. The SPPs are excited by few-cycle near-infrared pulses using Kretschmann coupling, and a nanotip is used as a local field sensor. This geometry removes the influence of the incident excitation laser from the near fields, and enhances the plasmon electric field strength. Using finite-difference-time-domain studies we show that the geometry can be used to measure SPP waveforms as a function of propagation distance. The effects of the nanotip shape and material on the field enhancement and plasmonic response are discussed.

©2016 Optical Society of America

OCIS codes: (000.0000) General; (000.2700) General science.

References and links

1. S. Nie and S. R. Emory, "Probing single molecules ans single nanoparticles by surface-enhanced Raman scattering," Science **275**(5303), 1102–1106 (1997).
2. R. F. Oulton, V. J. Sorger, D. A. Genov, D. F. P. Pile, and X. Zhang, "A hybrid plasmonic waveguide for subwavelength confinement and long-range propagation," Nat. Photonics **2**(8), 496–500 (2008).
3. E. Betzig and R. J. Chichester, "Single molecules observed by near-field scanning optical microscopy," Science **262**(5138), 1422–1425 (1993).
4. H. A. Atwater and A. Polman, "Plasmonics for improved photovoltaic devices," Nat. Mater. **9**(3), 205–213 (2010).
5. J. N. Anker, W. P. Hall, O. Lyandres, N. C. Shah, J. Zhao, and R. P. Van Duyne, "Biosensing with plasmonic nanosensors," Nat. Mater. **7**(6), 442–453 (2008).
6. N. Liu, M. Hentschel, T. Weiss, A. P. Alivisatos, and H. Giessen, "Three-dimensional plasmon rulers," Science **332**(6036), 1407–1410 (2011).
7. V. M. Shalaev, "Optical negative-index metamaterials," Nat. Photonics **1**(1), 41–48 (2007).
8. E. Ozbay, "Plasmonics: merging photonics and electronics at nanoscale dimensions," Science **311**(5758), 189–193 (2006).
9. A. Weber-Bargioni, A. Schwartzberg, M. Schmidt, B. Harteneck, D. F. Ogletree, P. J. Schuck, and S. Cabrini, "Functional plasmonic antenna scanning probes fabricated by induced-deposition mask lithography," Nanotechnology **21**(6), 065306 (2010).
10. M. Rycenga, C. M. Cobley, J. Zeng, W. Li, C. H. Moran, Q. Zhang, D. Qin, and Y. Xia, "Controlling the synthesis and assembly of silver nanostructures for plasmonic applications," Chem. Rev. **111**(6), 3669–3712 (2011).
11. M. A. Garcia, "Surface plasmons in metallic nanoparticles: fundamentals and applications," J. Phys. D Appl. Phys. **44**(28), 283001 (2011).
12. F. Süßmann and M. F. Kling, "Attosecond nanoplasmonic streaking of localized fields near metal nanospheres," Phys. Rev. B **84**(12), 121406 (2011).
13. J. L. West and N. J. Halas, "Engineered nanomaterials for biophotonics applications: improving sensing, imaging, and therapeutics," Annu. Rev. Biomed. Eng. **5**(1), 285–292 (2003).
14. W. A. Murray and W. L. Barnes, "Plasmonic Materials," Adv. Mater. **19**(22), 3771–3782 (2007).
15. J. Homola, S. S. Yee, and G. Gauglitz, "Surface plasmon resonance sensors: review," Sens. Actuators B Chem. **54**(1), 3–15 (1999).

#252410 Received 22 Oct 2015; revised 18 Dec 2015; accepted 22 Dec 2015; published 4 Jan 2016

16. J. J. Mock, D. R. Smith, and S. Schultz, "Local refractive index dependence of plasmon resonance spectra from individual nanoparticles," Nano Lett. **3**(4), 485–491 (2003).
17. G. Herink, D. R. Solli, M. Gulde, and C. Ropers, "Field-driven photoemission from nanostructures quenches the quiver motion," Nature **483**(7388), 190–193 (2012).
18. M. Krüger, M. Schenk, and P. Hommelhoff, "Attosecond control of electrons emitted from a nanoscale metal tip," Nature **475**(7354), 78–81 (2011).
19. B. Piglosiewicz, S. Schmidt, D. J. Park, J. Vogelsang, P. Groß, C. Manzoni, P. Farinello, G. Cerullo, and C. Lienau, "Carrier-envelope phase effects on the strong-field photoemission of electrons from metallic nanostructures," Nat. Photonics **8**(1), 37–42 (2013).
20. S. Zherebtsov, T. Fennel, J. Plenge, E. Antonsson, I. Znakovskaya, A. Wirth, O. Herrwerth, F. Süßmann, C. Peltz, I. Ahmad, S. A. Trushin, V. Pervak, S. Karsch, M. J. J. Vrakking, B. Langer, C. Graf, M. I. Stockman, F. Krausz, E. Rühl, and M. F. Kling, "Controlled near-field enhanced electron acceleration from dielectric nanospheres with intense few-cycle laser fields," Nat. Phys. **7**(8), 656–662 (2011).
21. F. Krausz and M. I. Stockman, "Attosecond metrology: from electron capture to future signal processing," Nat. Photonics **8**(3), 205–213 (2014).
22. P. Dombi, S. E. Irvine, P. Rácz, M. Lenner, N. Kroó, G. Farkas, A. Mitrofanov, A. Baltuška, T. Fuji, F. Krausz, and A. Y. Elezzabi, "Observation of few-cycle, strong-field phenomena in surface plasmon fields," Opt. Express **18**(23), 24206–24212 (2010).
23. J. Vogelsang, J. Robin, B. J. Nagy, P. Dombi, D. Rosenkranz, M. Schiek, P. Groß, and C. Lienau, "Ultrafast electron emission from a sharp metal nanotaper driven by adiabatic nanofocusing of surface plasmons," Nano Lett. **15**(7), 4685–4691 (2015).
24. T. Hanke, G. Krauss, D. Träutlein, B. Wild, R. Bratschitsch, and A. Leitenstorfer, "Efficient nonlinear light emission of single gold optical antennas driven by few-cycle near-infrared pulses," Phys. Rev. Lett. **103**(25), 257404 (2009).
25. A. Anderson, K. S. Deryckx, X. G. Xu, G. Steinmeyer, and M. B. Raschke, "Few-femtosecond plasmon dephasing of a single metallic nanostructure from optical response function reconstruction by interferometric frequency resolved optical gating," Nano Lett. **10**(7), 2519–2524 (2010).
26. C. Rewitz, T. Keitzl, P. Tuchscherer, J. S. Huang, P. Geisler, G. Razinskas, B. Hecht, and T. Brixner, "Ultrafast plasmon propagation in nanowires characterized by far-field spectral interferometry," Nano Lett. **12**(1), 45–49 (2012).
27. A. G. Borisov, P. M. Echenique, and A. K. Kazansky, "Attostreaking with metallic nano-objects," New J. Phys. **14**(2), 023036 (2012).
28. F. Kelkensberg, A. F. Koenderink, and M. J. J. Vrakking, "Attosecond streaking in a nano-plasmonic field," New J. Phys. **14**(9), 093034 (2012).
29. J. S. Prell, L. J. Borja, D. M. Neumark, and S. R. Leone, "Simulation of attosecond-resolved imaging of the plasmon electric field in metallic nanoparticles," Ann. Phys. **525**(1), 151–161 (2013).
30. E. Skopalová, D. Y. Lei, T. Witting, C. Arrell, F. Frank, Y. Sonnefraud, S. A. Maier, J. W. G. Tisch, and J. P. Marangos, "Numerical simulation of attosecond nanoplasmonic streaking," New J. Phys. **13**(8), 083003 (2011).
31. M. Lupetti, J. Hengster, T. Uphues, and A. Scrinzi, "Attosecond photoscopy of surface plasmon polaritons," http://arxiv.org/abs/1401.4290v1 (2014).
32. B. Förg, J. Schötz, F. Süßmann, M. Förster, M. Krüger, B. Ahn, K. Wintersperger, S. Zherebtsov, A. Guggenmos, V. Pervak, A. Kessell, S. A. Trushin, A. M. Azzeer, M. I. Stockman, D. Kim, F. Krausz, P. Hommelhoff, and M.F. Kling, "Attosecond nanoscale near-field sampling," http://www.arxiv.org/abs/1508.05611 (2015).
33. M. I. Stockman, M. F. Kling, U. Kleineberg, and F. Krausz, "Attosecond nanoplasmonic field microscope," Nat. Photonics **1**(9), 539–544 (2007).
34. S. H. Chew, F. Süßmann, C. Späth, A. Wirth, J. Schmidt, S. Zherebtsov, A. Guggenmos, A. Oelsner, N. Weber, J. Kapaldo, A. Gliserin, M. I. Stockman, M. F. Kling, and U. Kleineberg, "Time-of-flight-photoelectron emission microscopy on plasmonic structures using attosecond extreme ultraviolet pulses," Appl. Phys. Lett. **100**(5), 051904 (2012).
35. A. Mikkelsen, J. Schwenke, T. Fordell, G. Luo, K. Klünder, E. Hilner, N. Anttu, A. A. Zakharov, E. Lundgren, J. Mauritsson, J. N. Andersen, H. Q. Xu, and A. L'Huillier, "Photoemission electron microscopy using extreme ultraviolet attosecond pulse trains," Rev. Sci. Instrum. **80**(12), 123703 (2009).
36. Y. Gong, A. G. Joly, D. Hu, P. Z. El-Khoury, and W. P. Hess, "Ultrafast imaging of surface plasmons propagating on a gold surface," Nano Lett. **15**(5), 3472–3478 (2015).
37. M. Krüger, S. Thomas, M. Förster, and P. Hommelhoff, "Self-probing of metal nanotips by rescattered electrons reveals the nano-optical near-field," J. Phys. At. Mol. Opt. Phys. **47**(12), 124022 (2014).
38. L. Novotny and B. Hecht, *Principles of Nano-Optics* (New York: Cambridge University Press, 2006).
39. S. A. Maier, *Plasmonics: Fundamentals and Applications* (Springer, 2007).
40. D. M. Sullivan, *Electromagnetic Simulation Using the FDTD Method* (IEEE Press Series, 2000).
41. A. Taflove, *Computational Electromagnetics: The Finite-Difference Time-Domain Method* (Artech House, 2005).
42. S. D. Gedney, *Introduction to the Finite-Difference Time-Domain (FDTD) Method for Electromagnetics* (Morgan & Claypool, 2011).
43. Lumerical Solutions, Inc., http://www.lumerical.com/tcad-products/fdtd/
44. R. Olmon, B. Slovick, T. Johnson, D. Shelton, S.-H. Oh, G. Boreman, and M. Raschke, "Optical dielectric function of gold," Phys. Rev. B **86**(23), 235147 (2012).
45. E. D. Palik, *Handbook of Optical Constants of Solids, Vol. 3* (Academic Press, 1998).

#252410 Received 22 Oct 2015; revised 18 Dec 2015; accepted 22 Dec 2015; published 4 Jan 2016
© 2016 OSA

46. S. Thomas, G. Wachter, C. Lemell, J. Burgdörfer, and P. Hommelhoff, "Large optical field enhancement for nanotips with large opening angles," New J. Phys. **17**(6), 063010 (2015).
47. C. Balanis, *Antenna Theory: Analysis and Design*, 3rd ed. (John Wiley & Sons, 2005).
48. C. C. Wu, K. L. Ou, and C. L. Tseng, "Fabrication and characterization of well-aligned and ultra-sharp silicon nanotip array," Nanoscale Res. Lett. **7**(1), 120 (2012).
49. G. S. Huang, X. L. Wu, Y. C. Cheng, X. F. Li, S. H. Luo, T. Feng, and P. K. Chu, "Fabrication and field emission property of a Si nanotip array," Nanotechnology **17**(22), 5573–5576 (2006).
50. T. C. Cheng, J. Shieh, W. J. Huang, M. C. Yang, M. H. Cheng, H. M. Lin, and M. N. Chang, "Hydrogen plasma dry etching method for field emission application," Appl. Phys. Lett. **88**(26), 263118 (2006).
51. C. H. Hsu, H. C. Lo, C. F. Chen, C. T. Wu, J. S. Hwang, D. Das, J. Tsai, L. C. Chen, and K. H. Chen, "Generally applicable self-masked dry etching technique for nanotip array fabrication," Nano Lett. **4**(3), 471–475 (2004).

1. Introduction

Since their discovery in the 1950s, surface plasmon polaritons (SPPs) have been used in a broad range of applications including surface-enhanced Raman scattering [1], wave-guiding [2], nanoscopy i.e. optical microscopy well below the diffraction limit [3], light trapping for enhanced solar energy conversion [4], chemical and bio-sensing [5], plasmon rulers [6], metamaterials [7], and plasmonic circuits [8]. This progress has been fueled by advances in fabrication techniques such as lithography [9] and chemical synthesis [10], where optical properties of nanomaterials are used to achieve functionality [11]. The properties of the collective dynamics depend on the laser field [12], the material composition [13], shape [14], configuration [9], the local environment of the nanotarget [15, 16]. Surface plasmons can concentrate light fields into extremely localized nanoscale volumes, allowing access to interesting new regimes of strong field physics [17], and steering of electron emission, acceleration and scattering processes at nanotips [18, 19] and nanoparticles [20].

Collective plasmonic electron dynamics evolve on few- to sub-femtosecond timescales. Tracing these dynamics on their natural nanometer-spatial and few-femtosecond temporal scales will allow optimization of ultrafast plasmonic dynamics for strong field physical processes, and control of plasmons for applications in new areas such as lightwave electronics [21]. Furthermore, an improved understanding of the fundamental physics involved in plasmon excitation, propagation and dephasing will be useful to plasmonic research and technology in general. A number of femtosecond techniques, based on autocorrelation [22, 23], frequency-resolved optical gating [24, 25], and spectral interferometry [26], have been developed in this direction. Attosecond streaking is expected to reveal the temporal structure of plasmons with attosecond resolution [12, 27–32] and, when combined with photoelectron-emission microscopy (PEEM), nanometer spatial resolution [33–35]. Time resolved PEEM of SPP dynamics has recently been demonstrated in the femtosecond domain [36].

In this paper, we analyze and discuss a technique for temporally characterizing SPPs as a function of propagation distance. Our approach is based on the use of a nanotip on thin Au film as local sensor for SPPs.

2. Approach

Figure 1 shows the scheme for utilizing nanotips as local field sensors for SPPs. In the geometry shown in Fig. 1, unlike other schemes of attosecond nanoplasmonic streaking [12, 30–32], the electrons' energy shift is not influenced by the incident near-infrared (NIR) laser field. None of the proposed schemes for probing SPPs using attosecond streaking proposed so far can fully separate the incident laser field from the SPP, because the incident excitation pulse occupies the same spatial region as the initial SPP, and because the SPP has only a weak field enhancement relative to the incident field, typically in the range of 0.5-1.5. Both fields would have a comparable effect in a streaking experiment, and the initial SPP at the excitation point cannot therefore be studied independently from the incident field. Furthermore the field strength of SPPs decays exponentially as they propagate. The fidelity of a field characterization using attosecond streaking depends on the field strength, limiting the propagation range over which the technique can be applied.

Our proposed geometry uses Kreschmann coupling to screen the incident excitation field, while a tip enhances the plasmonic field strength. The proposed geometry is thus adequate for

#252410 Received 22 Oct 2015; revised 18 Dec 2015; accepted 22 Dec 2015; published 4 Jan 2016
© 2016 OSA

tracing transient surface plasmon polaritons with attosecond precision, for a wider range of propagation distances including the initial excitation point, free from effects of the incident excitation field.. Other schemes to obtain information about nanolocalized fields, for example the maximum field strength, from strong field photoemission alone have been proposed [37]. Here, we go beyond these studies and focus on the relation of LSPs at the nanotip to the propagating SPPs.

A linearly polarized, few-cycle NIR laser pulse is launched to a 50 nm gold film on a SiO_2 right-angle prism at an angle of incidence of 45 degree in order to induce propagating surface plasmon polaritons.

The depicted SPP excitation scheme is well-known as the Kretschmann configuration. SPPs can be efficiently excited when the incident and surface plasmon wave vectors satisfy the condition: $\Re(k_i) = \Re(k_p)$, where $\Re$ indicates the real part, $\boldsymbol{k}_i$ is the parallel component of the wave vector of the incident light to the prism interface,

$$k_i = \left(\frac{2\pi}{\lambda}\right) n \sin\theta, \tag{1}$$

θ is the incident light angle, λ is the wavelength, and n is the refractive index of the prism. The wave number of the plasmon mode along the interface is given by:

$$k_p = \left(\frac{2\pi}{\lambda}\right)\sqrt{\frac{\varepsilon_1\varepsilon_2}{\varepsilon_1+\varepsilon_2}}, \tag{2}$$

where ε_1 and ε_2 are the dielectric permittivities of the metal film and the dielectric medium above the surface, respectively. Efficient SPP excitation gives rise a well-defined minimum in the intensity of the reflected light [38]. For monochromatic plane waves, an analytic solution for the SPP excitation in terms of Fresnel coefficients is available [39], which is, however, not applicable to the broadband focused beams in this paper. We calculated that the peak field strength of the NIR laser pulse transmitted through the film is less than 0.8% of the peak SPP field strength, and the incident excitation pulse therefore has a negligible contribution to the near-fields in the region of the initial SPP waveform.

Additionally, on the prism, a conical gold nanotip having suitable dimensions is placed in a position where the field strength of the SPP is at its maximum. The nanotip serves as an efficient local field sensor by transforming the SPP into a stronger nano-localized surface plasmon (LSP) at the tip apex as shown in Figs. 1(a) and 1(b). The local field generated at the apex is spatially confined and enhanced with respect to both the incident NIR and SPP fields.

The near-field of the LSP at the nanotip exponentially decays along the *z*-axis into the vacuum as depicted in Fig. 1(c). The nanotip near-field can be probed by e.g. attosecond streaking, where an attosecond extreme ultraviolet pulse frees electrons from the surface of the tip that are accelerated in the near-field [27–33]. The measurement of electron momentum as a function of delay time between the extreme ultraviolet pulse and the exciting NIR pulse permits, under suitable conditions, the retrieval of the near-field [33].

Regarding to the spatial distribution of the fields around the tip, it is inhomogeneous and localized as shown in Fig. 1(c). Hence all the accumulated signals from the SPP would be confined at the apex and then appropriately reflected in the streaking measurement. Therefore the main contributions to the streaking trace will mostly come from the field at the apex. This means that we can get useful information about the field of the propagating SPP on a metal film by utilizing it as an efficient local field sensor.

#252410 Received 22 Oct 2015; revised 18 Dec 2015; accepted 22 Dec 2015; published 4 Jan 2016
© 2016 OSA

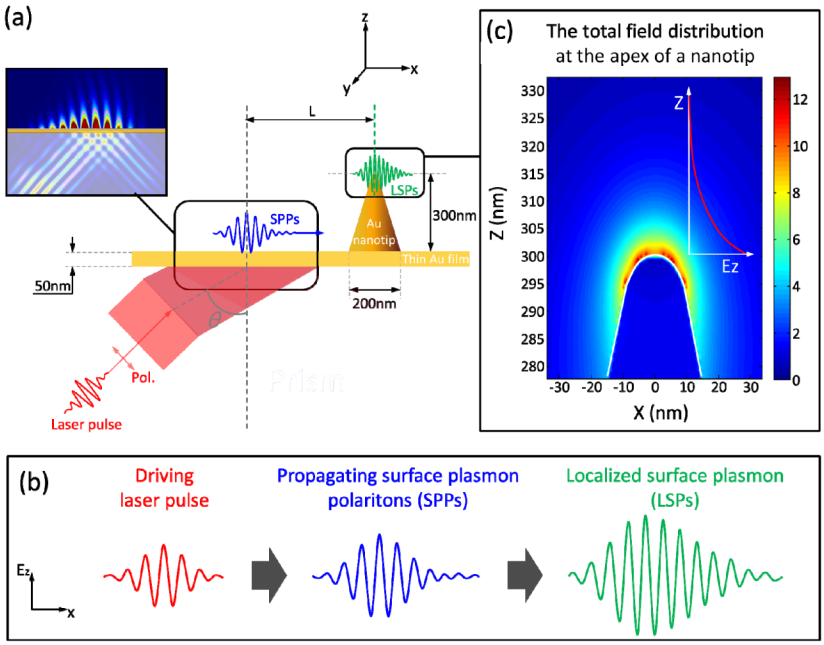

Fig. 1. A linearly polarized, few-cycle NIR laser pulse is launched to a 50 nm gold film on a SiO_2 right-angle prism at an angle of incidence of 45 degree in order to induce propagating surface plasmon polaritons. (a) Scheme for locally confined fields at the end of a metal nanotip excited by propagating surface plasmons. The inset shows the near-field distribution near the metal film. (b) The configuration of light-SPP coupling and induced dipole coupling on a nanotip. The quantity plotted shows a maximum instantaneous field enhancement. (c) Field distribution at the nanotip apex. The inset shows the maximum of the time-integrated electric field component along the tip axis.

3. Optimization of the nanotip geometry

We have carried out simulations to optimize the nanotip geometry and identify ideal conditions for coupling the propagating surface plasmon to the localized plasmon at the nanotip apex. The incident laser pulse at 720 nm with 4.5 fs duration (full-width-at-half-maximum of its Gaussian intensity profile) is linearly polarized as shown in Fig. 1(a). In order to calculate the time-dependent plasmonic fields, we employed finite-difference-time-domain (FDTD) simulations [40–42]. A commercial software package, Lumerical FDTD Solutions 2015b (v8.12.527) [43], was used to perform the calculations. The real and imaginary parts of the wavelength-dependent dielectric functions for gold and fused silica were taken from Olmon's data and Palik's data respectively [44, 45]. The surface of the glass (silicon dioxide, SiO_2) prism (index of refraction $n = 1.45$) is covered by gold and the nanotip is surrounded by vacuum (index of refraction $n = 1$). The total simulation region was set to $8.8 \times 3.0 \times 5.6$ μm^3. A perfectly-matched layer boundary condition with a thickness of 380 nm is applied to minimize reflections of outgoing fields at the boundary of the simulation region. To ensure an accurate description of the near-field of the nanotip, a three-dimensional adaptive fine mesh with a unit size of $0.5 \times 0.5 \times 0.5$ nm^3 was used in the area of the apex and the entire simulation volume was divided by a uniform mesh of $8.0 \times 8.0 \times 8.0$ nm^3. The total time window for the simulation was 120 fs with a time step of 1 as.

Before carrying out the simulation for optimization of the geometry, we investigated the SPP excitation, which also affects the choice of nanotip position. Figure 2(a) shows a decaying behavior of a propagating SPP at different points along the gold surface. As the SPP propagates along the surface, it loses energy due to absorption in the metal and due to

#252410 Received 22 Oct 2015; revised 18 Dec 2015; accepted 22 Dec 2015; published 4 Jan 2016
© 2016 OSA

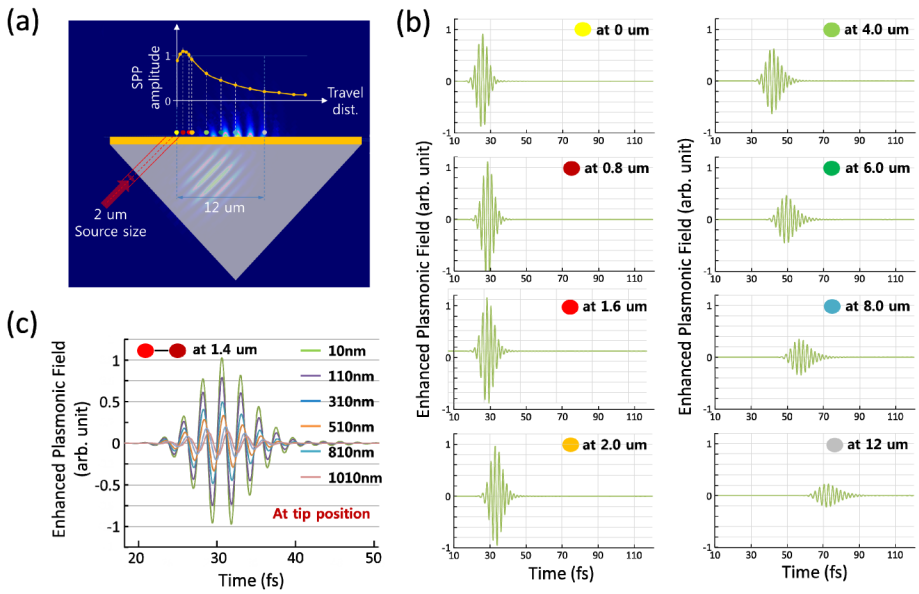

Fig. 2. Decaying behavior of the propagating SPPs on the gold surface (a) and their field waveform along the surface at different positions (b), and the height at a fixed position on the surface (c). All the colored dots in (b) and (c) indicate the relevant positions on the surface in (a). The tip on the surface is at a distance of 1.4 um from the center of the excitation laser pulse as indicated in (c).

scattering into free-space. Remarkably, the maximum plasmon field occurs outside the region of the incoming excitation, here at a distance of about 800 nm from the center point of its excitation (dark red in Fig. 2(a)). Then the field dissipates to less than 20% of the peak SPP field strength after traveling 12 µm as shown in Fig. 2(b) and to below 1% after traveling 40 µm which is comparable with the usual plasmon decay length of about 50 µm, given by the imaginary part of Eq. (2). The change of the SPP electric field at different distances from the surface is shown in Fig. 2(c). With increasing distance, the SPP electric field changes in amplitude as expected due to the localization of the SPP to the surface. For our simulations, we placed the nanotip at a distance of 1.4 um from the center of the excitation laser pulse.

A series of simulations have been carried out for different height, diameter of the conical tip's base, and apex radius of curvature in order to optimize the field enhancement at the apex for the condition that the nanotip serves as a sensor of the SPP. The results are shown in Fig. 3. As shown in Fig. 3(a), the smaller the radius of a nanotip (R), the larger the field enhancement. A similar curve has recently been found for single nanotips excited by a free-propagating laser beam [37]. The universality of this curve is a consequence of geometric field enhancement, in analogy to the lightning rod effect of electrostatics. Considering the fabrication of a sharp tip, R = 10 nm was chosen as a typical apex parameter. For a fixed height of H = 300 nm, the base diameter D was optimized for maximum field enhancement, where D = 200 nm yielded the highest field enhancement. The resulting opening angle of around 18° is in agreement with a recent study on the opening angle dependence of field enhancement on single tips and is connected to the excitation of a plasmon along the nanotip shaft [46]. Subsequently, the height of the nanotips was optimized for a fixed apex radius (10 nm) and base diameter (200 nm). In classical antenna theory for the given configuration, antenna on a ground plate, the maximum enhancement with respect to the input field would be expected for an antenna length of one quarter of the wavelength of the exciting light [47]. Surprisingly in the simulations it occurs at bigger heights of around 300 nm, although the SPP is decreasing with increasing distance from the surface. Indeed the observation of the

#252410 Received 22 Oct 2015; revised 18 Dec 2015; accepted 22 Dec 2015; published 4 Jan 2016
© 2016 OSA

resonance angle already indicates more complex dynamics, which is not accounted for in classical radio frequency (RF) theory.

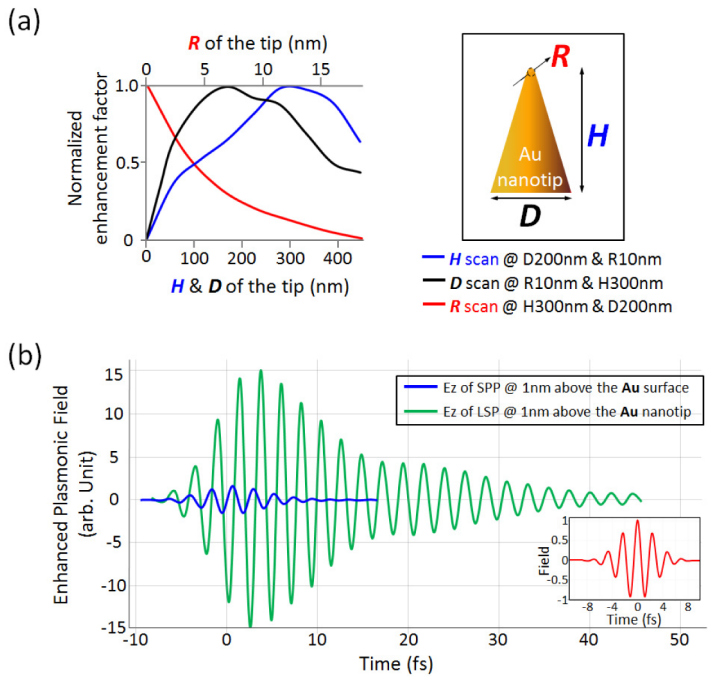

Fig. 3. (a) Optimal shape of a conical gold nanotip. The inset shows the schematics of the nanotip. The quantity plotted shows a maximum instantaneous field enhancement. (b) Comparison of the time-dependent plasmonic field profile between SPP & LSP in resonant condition at the apex of the conical gold nanotip. The height, H, of 300 nm, the bottom diameter, D, of 200 nm and a radius of curvature, R, of 10 nm were chosen for the nanotip. The plasmonic field enhancement at a point of 1 nm above the tip and the gold surface, respectively, (with respect to a normalized laser field) is calculated via FDTD simulations. The inset in (b) shows the temporal profile of the driving laser pulse. The laser field has been normalized to 1.

A conical nanotip with a height of 300 nm, a base diameter of 200 nm and a radius of curvature at the tip of 10 nm was found to provide resonant enhancement of the SPP. Figure 3(b) shows the temporal profile of the LSP field (green line) at a point 1 nm above the nanotip The blue-line in Fig. 3(b) shows the temporal profile of the SPP field at a point 1 nm above the 50 nm gold film on the prism without a nanotip. The inset shows the temporal profile of the incident laser field used in this simulation. The maximum field enhancement at the tip apex was approximately 15 with respect to the normalized incident laser field in the *z*-component of the plasmonic field Ez(*x*,*z*) along the tip axis and the field enhancement factor of the SPP at the same position was 1.25. The LSP temporally lasts for more than 40 fs. While the LSP increases the field amplitude of the SPP for easier probing by e.g. attosecond streaking, the temporal field profile of the LSP differs noticeably from that of the SPP. A full understanding of the near-field properties and dynamics of SPPs would require detailed information about its sub-cycle evolution, from attosecond streaking measurements, for example.

As the LSP electric field in 3 (b) differs substantially from the SPP temporal structure, we now turn our attention to other nanotip materials, where the probing step is performed under non-resonant conditions. We have investigated a number of metals and semiconductors for this purpose, including Ag, Pt, Cu, W, Ge, GaAs and Si. The optical properties were obtained from Palik's data [45]. The FDTD simulations were performed in a discrete, non-uniformly spaced mesh with a resolution of below 4 nm and 0.5 nm in a region of fine meshes. The most

#252410 Received 22 Oct 2015; revised 18 Dec 2015; accepted 22 Dec 2015; published 4 Jan 2016
© 2016 OSA

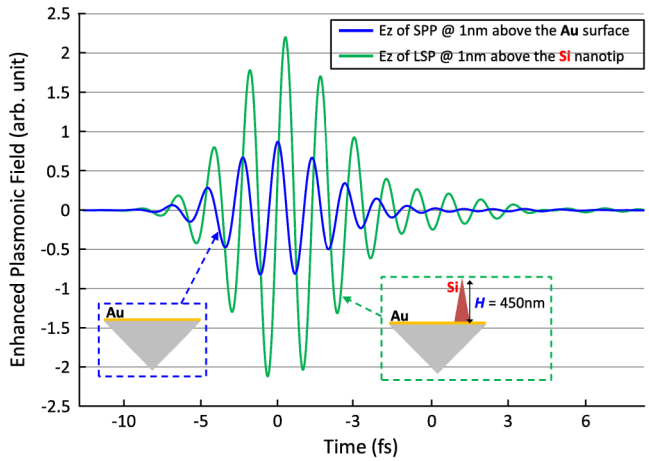

Fig. 4. Comparison of the temporal profile and the plasmonic field enhancement between the LSP for a Si nanotip with H = 450 nm, D = 200 nm and R = 10 nm (green line) and the SPP without a nanotip (blue line) at a field monitor point, 1 nm above the tip and gold surface, respectively.

direct mapping of the SPP field was found using Si as the nanotip material, with H = 450 nm, D = 200 nm and R = 10 nm, as shown in Figs. 4 and 5.

In the off-resonant case, we observe a substantially improved qualitative agreement between the temporal structures of the SPP and LSP fields. In order to quantitatively understand the relationship between the SPP and the LSP, we analysed the pulses in the spectral domain, as shown in Fig. 5(a) and 5(b). A fourth-order polynomial nonlinear least squares fit to the spectral phase was used to determine the carrier-envelope phase (CEP, φ_0), the group delay dispersion (φ_2), and the third (φ_3) and fourth (φ_4) order dispersion. The fitted phase coefficients, as well as the central frequency (ω_0) and full-width half-maximum duration of the intensity envelope (τ) are summarized in Table 1 for both the SPP and the LSP.

The main difference between the LSP and SPP is a simple CEP shift of (0.432 ± 0.009) π rad. Changing H by ± 10 nm (at fixed D = 200 nm) changes this shift by less than ± 0.03 π rad, corresponding to a temporal change of 33 attoseconds (as) at the SPP central wavelength of 670 nm. Changing D in 5 nm steps from 190 nm to 210 nm changes the CEP shift by less than ± 0.04 π rad, corresponding to 45 as. As the CEP shift is robust to slight changes in nanotip dimensions, it is predictable and can be corrected for when analyzing experimental results.

Apart from the CEP shift, the LSP and SPP temporal structures are in good agreement, as shown in Fig. 5(c), with the other differences being a slight shift in central frequency of 4×10^{13} rad s^{-1} (corresponding to a central wavelength shift of approximately 10 nm), and a low amplitude tail at around 10 fs which separates into a small post-pulse for some combinations of H and D. Replacing the φ_2, φ_3, and φ_4 phase coefficients of the LSP with the corresponding SPP phase coefficients did not remove the tail. We therefore attribute this feature either to small amounts of higher order phase, or to the slightly larger temporal Fourier-limit of the LSP (5.5 fs) compared to that of the SPP (5.1 fs).

The simulated LSPs contain a sub-structure below 10% of the peak electric field at times >15fs after the pulse center, which is the origin of the interference fringes visible in the LSP spectrum in Fig. 5(b). This sub-structure is a bit sensitive in phase and amplitude to the spatial size of the simulation window but it is clearly not an artefact of the simulation. It comes from its incident self-resonance behaivor after interacting with the SPP as a minor effect for Si. We believe that it can be minimized by tuning the tip's shape more and also can be subtracted

#252410 Received 22 Oct 2015; revised 18 Dec 2015; accepted 22 Dec 2015; published 4 Jan 2016
© 2016 OSA

from the experimental steaking result computationally in order to reach a better agreement in its analysis.

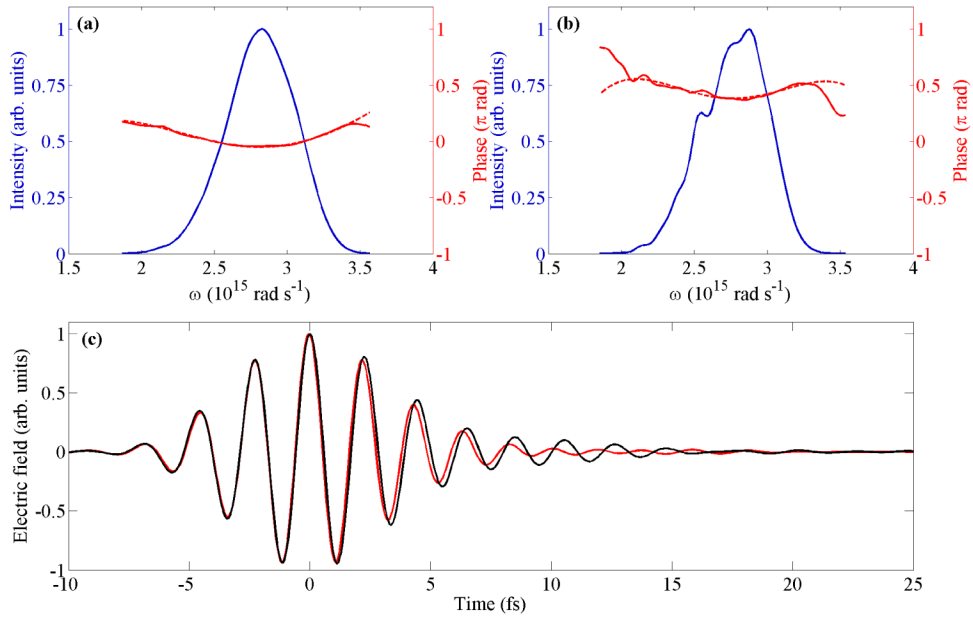

Fig. 5. (a) SPP spectral intensity (solid blue), phase (solid red), and fitted phase (dashed red). (b) LSP spectral intensity (solid blue), phase (solid red), and fitted phase (dashed red) for Si nanotip with H = 450 nm, D = 200 nm and R = 10 nm. The fitted linear terms (corresponding to a time delay) have been subtracted in (a) and (b) from the phase and the fitted phase. (c) Normalized SPP (red) and LSP (black) electric fields. The fitted CEPs and linear phases have been subtracted from both the SPP and LSP in (c), and the LSP has been delayed by an additional 0.28 fs.

Table 1. Comparison of SPP and LSP central frequency, duration, and fitted spectral phase coefficients for Si nanotip with H = 450 nm, D = 200 nm and R = 10 nm. The errors in the fitted spectral phase coefficients are the 95% confidence intervals of the fit.

	ω_0 (10^{15} rad s^{-1})	τ (fs)	φ_0 (π rad)	φ_2 (fs^2)	φ_3 (fs^3)	φ_4 (fs^4)
SPP	2.81	5.2	–0.049 ± 0.002	3.4 ± 0.2	2.5 ± 0.6	–13 ± 5
LSP	2.77	5.6	0.383 ± 0.007	4.8 ± 0.7	–0.7 ± 2	–69 ± 24

In summary, the temporal structures of the LSP of an off-resonant nanotip and that of the SPP are in good agreement, implying that an off-resonant nanotip can be used as a local sensor. Hence it can be used to characterize the SPP as a function of the propagation distance.

As shown in Fig. 4, the LSP field is enhanced with respect to the SPP field by about a factor of 2.2. While this field enhancement is relatively modest, it is nevertheless advantageous because of the short propagation lengths of SPPs. The field strength of an SPP decays exponentially with a characteristic distance L as it propagates away from its excitation point. There is typically a minimum field strength required for a robust field characterization in an attosecond streaking experiment. An enhancement factor of 2.2 increases the propagation length over which the field strength will remain sufficient for streaking by L ln(2.2), thereby increasing the propagation range over which the SPP can be studied. In order to avoid background from the plain gold film, the XUV beam should be propagated at a shallow angle to the surface, in such a position that it illuminates only the tip. Sample positioning could be performed by measuring the count rate of photoelectrons emitted by the XUV as a function the sample position, as demonstrated experimentally in Förg et al. [32]. With further optimization of the probe antenna, using for example composite materials and different geometries, it should be possible to improve the field enhancement factor further.

#252410 Received 22 Oct 2015; revised 18 Dec 2015; accepted 22 Dec 2015; published 4 Jan 2016
© 2016 OSA

While streaking traces from nanostructured samples can be rather complex [27–31], it has already been demonstrated experimentally that local near fields surrounding nanotips can be characterized using attosecond streaking [32] and Si nano-tip on Au substrate is technically available by exploiting the fabrication processes which was already demonstrated by several groups [48–51]. In detail, the Si-Au-SiO_2 substrate can be made by e-beam or thermal evaporation of Au and SiO_2 sequentially on Si wafer. The single or multiple silicon nano tip on Au substrate could be made by selective plasma dry etching on the back side of Si wafer after making small photoresist pattern on Si. The time of plasma dry etching determines not only to make a Si nano tip shape also to eliminate residual Si substrate on Au film excepting the Si nano tip. Finally, the Si nano tip on Au substrate could be fabricated for plasmonic streaking experiment [48].

We therefore expect our proposed geometry to be ameanable to this technique. A key advantage of using the Si tip is that it serves as a local probe of the SPP field with sub-micrometer resolution and provides a direct measurement of the field evolution.

4. Conclusions

Collective electron dynamics, such as localized and propagating surface plasmons have been theoretically investigated for a nanotip on surface. By a comparison of the temporal behaviors of the field oscillation, enhancement factor and overall exponential decay lengths of the enhanced plasmonic fields, we identify resonant and non-resonant conditions for the probing of SPPs using a different material of the tip under given excitation conditions. We proposed an experimental geometry which is adequate for tracing transient surface plasmon polaritons using attosecond streaking spectroscopy without any direct influence by the NIR laser field on the electron acceleration process.

5. Acknowledgement

We are grateful to E. Goulielmakis and F. Krausz for support within the framework of the Max Planck Center for Attosecond Science (MPCAS). We acknowledge support by the Max Planck Society, the DFG via the Cluster of Excellence: Munich Center for Advanced Photonics (MAP) and the EU via the ERC grant ATTOCO. B.F. and M.F.K. are grateful for support by the competitive research funding from King Abdullah University of Science and Technology (KAUST). B.A., S.C.K., and D. K. acknowledge that this research has been supported in part by Global Research Laboratory Program [Grant No 2009-00439] and by Max Planck POSTECH/KOREA Research Initiative Program [Grant No 2011-0031558] through the National Research Foundation of Korea (NRF) funded by Ministry of Science, ICT & Future Planning.

© 2016 OSA